Tellus (1995), 47A, 892–910
Printed in Belgium – all rights reserved

TELLUS
ISSN 0280-6495

Estimating divergence and vorticity from the wind profiler network hourly wind measurements

By J. L. LEE,[1*,2] G. L. BROWNING[1,3] and Y. F. XIE[3], [1]*NOAA/ERL Forecast Systems Laboratory R/E/FS, 325 Broadway, Boulder, Colorado, 80303, USA*; [2]*STC, Hampton, Virginia 23666, USA*; [3]*CIRA, CSU Foothills Campus, Fort Collins, Colorado, 80523, USA*

(Manuscript received 10 August 1994; in final form 29 March 1995)

ABSTRACT

The large-scale horizontal divergences computed from the kinematic and vorticity methods based on a four-dimensional least squares fit (4-D LSF) to the hourly wind measurements from the Wind Profiler Demonstration Network (WPDN) are compared to the divergence derived from a four-dimensional data assimilation (4-DDA) system. The kinematic method computes divergence by adding the appropriate terms of the velocity derivatives, while the vorticity method uses the dynamical balance of terms in the vorticity equation. The 4-D LSF method produces wind and vorticity analyses by approximating the analyzed wind field as a series of basis functions dependent on both space and time. The sensitivity of the basis functions is studied with an analytic solution and with real data. It is shown that the LSF results are not sensitive to the choice of basis functions as long as they include adequate variation to resolve the data. The high temporal resolution divergence and vorticity fields, which are obtained directly from hourly WPDN data, are used to independently validate the 4-DDA derived vorticity and divergence, which depend both on observational data and on the dynamics and physics in data assimilation models. For the initial case study, the relative errors between the 4-D LSF or the 4-DDA analysis and the WPDN measurements are essentially the same, and the smooth parts of the vorticity derived from these two analyses are similar. The large-scale divergence derived from the vorticity method is also in good agreement with that derived from the 4-DDA analysis. However, the divergence derived from the kinematic method shows little resemblance to those derived from the vorticity method and 4-DDA analysis.

1. Introduction

Horizontal divergence is one of the most important dynamical quantities in weather forecasting and atmospheric research. For example, horizontal divergence in the upper troposphere induces low level convergence resulting in severe weather outbreaks (Beebe and Bates, 1955). The failure to correctly determine the initial horizontal divergence in weather prediction models is partially responsible for the spin-up problem in short-term precipitation forecasting (Kasahara et al., 1992). The divergence field has been used to derive realistic large-scale distributions of atmospheric heat sources and sinks (Sardeshmukh, 1993). Horizontal divergence can be inferred dynamically from the vorticity variations in space and in time based on the vorticity equation. This method is referred to as the vorticity method (Sawyer, 1949). The vorticity method was applied successfully by Eliassen and Hubert (1953) to infer vertical motions in a blocking weather situation where the local time changes are small and unimportant. Recently, Sardeshmukh (1993) applied the vorticity method to global data analyzed at the European Centre for Medium-Range Weather Forecasts (ECMWF) and suggested several improvements over the diabatically initialized ECMWF analysis. However, he necessarily computed climatological mean divergence fields

* Corresponding author.

because of the lack of high temporal resolution global analysis data.

The National Oceanic and Atmospheric Administration (NOAA) Wind Profiler Demonstration Network (WPDN) was established to provide high temporal resolution hourly wind measurements with a horizontal resolution of approximately 250 km over the central United States (see Fig. 1 for site locations). With the advent of WPDN hourly data, the main purpose of this paper is to use the vorticity method in conjunction with WPDN high temporal resolution data to derive the large-scale divergence and vorticity fields. These high temporal resolution divergence and vorticity fields are compared with those derived from the kinematic method and the four-dimensional data assimilation (4-DDA) system. The kinematic method (Bellamy, 1949) computes horizontal divergence by directly adding the appropriate components of the spatial derivatives of the velocity. In a 4-DDA system (Bengtsson, 1982), a weather forecast model is numerically integrated in time and observations are inserted into the model whenever they are available.

Errors in the horizontal divergence derived from the vorticity and kinematic methods were analyzed by Lee and Browning (1994), hereafter referred to as LB. They showed that the error in the divergence derived from the vorticity method is comparable to that in the wind measurements, while in the kinematic method the observational error is amplified by the reciprocal of the Rossby number. In contrast, a direct error analysis of the divergence derived from a 4-DDA system is very difficult because it is the product of both a complicated data assimilation model and the observational data. The error analysis of a 4-DDA system is usually undertaken by using numerical model simulations (Daley and Mayer, 1986). These experiments typically consist of taking "observations" at points corresponding to the global observational network from the output of one model considered to be the real atmosphere to produce an analyzed data set. The analyzed data set is then used as the initial data for a different model and the output from that model is compared to the output from the control run. There are obviously a number of concerns about such a comparison. For example, the control run is not the real atmosphere and all models have similar dynamics and physics, i.e., the twin experiment problem. Clearly an independent confirmation of the validity of the 4-DDA analysis without these problems is desirable.

This study produces such an independent means of validating the 4-DDA analysis by comparing its dynamical fields, in particular the large-scale horizontal divergence, with those derived directly from high temporal resolution wind measurements. The viability of the large-scale divergence derived from the vorticity method based on the wind profiler network was shown by LB. Following the analysis in that study, only the large-scale motions which are spatially resolved by the WPDN are considered in this study. The remaining question in a practical application of the vorticity method is how to obtain WPDN wind analyses on a regular grid mesh from the irregularly distributed WPDN observations.

The least squares fit (LSF) method has been used to achieve the above goal in analyzing meteorological data. A LSF method represents the analyzed field as a series of analytic basis functions whose coefficients are determined by minimizing the difference between the observational data and a series of functions. Panofsky (1949), Gilchrist and Cressman (1954), Dixon et al. (1972), Wahba and Wendelberger (1980), and Halberstam and Tung (1984) applied LSF techniques with time independent basis functions. Sasaki (1969), Lewis (1972), Talagrand and Courtier (1987), Derber (1987) and others extended the variational problem to include time using numerical models as constraints. With the availability of the hourly profiler data, we have developed a four-dimensional least squares fit (4-D LSF) method including time dependent basis functions to directly fit the high temporal WPDN data.

The vorticity method derives the large-scale divergence from the 4-D LSF analyzed wind and vorticity fields. The vorticity and 4-D LSF methods are tested with an analytic solution, and then are applied to the WPDN data for a 24-h period. The WPDN results are compared with those derived from the 4-DDA analysis used in the National Meteorological Center (NMC) global data assimilation system (GDAS) (Kanamitsu, 1989; Parrish and Derber, 1991). Since GDAS does not assimilate WPDN data and the 4-D LSF results are derived solely from the hourly WPDN data, comparisons of these two independent analyses will not be clouded by the aforementioned twin experiment problem.

Section 2 describes the vorticity and the 4-D LSF methods. Numerical tests of the 4-D LSF method using an analytic solution are given in Section 3. Section 4 shows the application of the vorticity method based on the 4-D LSF of the WPDN data and the results are compared with GDAS analysis data. Finally, conclusions are given in Section 5.

2. Numerical methods

In a periodic domain, shortwave observational noise can be removed by Fourier transforming the data and truncating the high wavenumbers. However, in the WPDN regional area, the data are in general non-periodic. The 4-D LSF method extends the Fourier decomposition technique to more general situations where the analyzed function is non-periodic. The 4-D LSF method derives a smooth wind field on a regular model grid mesh from the irregularly distributed WPDN hourly wind measurements. The derived wind values on a regular grid are used to numerically compute the vorticity and divergence from the vorticity method. The numerical technique used for the vorticity method is adopted from the bounded derivative principle (Kreiss, 1980; Browning et al., 1980) and is described in detail in LB. For the purpose of comparisons, the kinematic method is also used to compute the divergence from the fitted wind field. The kinematic method is well known (Bellamy, 1949; Schaefer and Doswell, 1979). The vorticity method although discussed intensively in LB is summerized here before the description of the 4-D LSF method.

2.1. The vorticity method

Vorticity variations in time and space can be used to derive the horizontal divergence in the midlatitudes through the vorticity equation. In the present study, we focus only on large-scale motions and compute the large-scale divergence from the quasi-geostrophic (Q–G) vorticity equation. The use of the Q–G vorticity equation in conjunction with the WPDN data has been justified in LB based on the average spacing of the WPDN stations.

Based on the Q–G vorticity equation, the large-scale horizontal divergence can be expressed as follows:

$$\nabla_{\mathrm{h}} \cdot V_{\mathrm{h}} = -\frac{1}{f+\zeta}\left(\frac{\partial}{\partial t}+u\frac{\partial}{\partial x}+v\frac{\partial}{\partial y}\right)(f+\zeta), \tag{1}$$

where the horizontal component of wind is $V_{\mathrm{h}} = (u, v, 0)$ and the horizontal gradient operator is defined as $\nabla_{\mathrm{h}} = (\partial/\partial x, \partial/\partial y, 0)$. The divergence and vorticity are defined as $\nabla_{\mathrm{h}} \cdot V_{\mathrm{h}}$ and $\zeta \equiv \partial v/\partial x - \partial u/\partial y$, respectively, and f is the Coriolis parameter. The Q–G vorticity equation requires that a change in the vorticity be accompanied by a change in the horizontal divergence. The large-scale horizontal divergence derived from the vorticity method is less sensitive to small errors in the horizontal wind than the kinematic method (see LB).

2.2. The 4-D LSF method

The LSF method approximates the analyzed field as a series expansion of basis functions. The selection of the basis functions should be based on the variability of the true data and noise. Since the variability in meteorological data are unknown a priori, we have tested a number of LSF techniques in order to choose appropriate basis functions for the WPDN data over a regional area. The shortcoming of choosing some commonly used orthogonal basis functions, e.g., spherical harmonics, is due to the small size of the area covered by the WPDN compared to the entire globe. For example, the zonal wavenumber corresponding to the domain of interest shown in Fig. 1 would require that the number of spherical harmonic basis functions exceed the number of profiler stations. Thus, the 4-D LSF method becomes an overfitting problem with too many basis functions. Consequently, the 4-D LSF could not remove noise from the data.

With the aforementioned difficulty, several LSF methods including constrained thin-plate and regular LSF splines have been examined. The thin-plate splines method (Wahba and Wendelberger, 1980) selects smoothing parameters via the Generalized Cross Validation algorithm. Both LSF splines packages were obtained from the NCAR software library. These LSF techniques were tested with an analytic solution and random

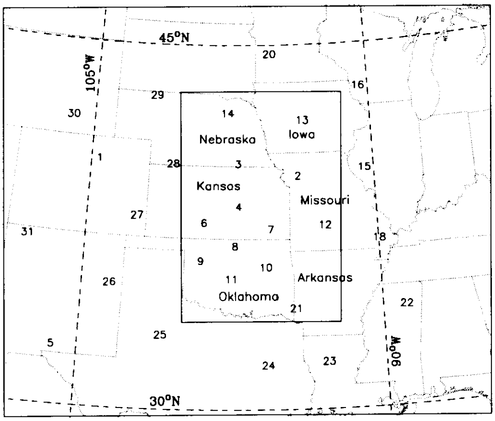

Fig. 1. Locations of the WPDN profiler sites and boundary of the window used for evaluating the analysis. The station numbers indicate profiler locations.

errors in the manner described in Section 3. The analytic test results from the thin-plate splines method showed that this method allowed too much variation in derivative quantities such as the vorticity and its gradient, i.e., the amount of noise in the fit caused large errors in high derivatives. In addition, the package available for this method required costly computations of $O(n^3)$, where n is the number of observations (Gu, 1989). For a 24-h period of WPDN data, the size of n is on the order of 10^4 which is too large to effectively apply the thin-plate spline to our applications.

For the case of regular LSF splines, we found that too many knots in the WPDN domain is equivalent to allowing too much variation in the basis functions. Apparently, the optimum number of knots in the LSF splines method should depend on the size of the domain of interest, e.g., the larger the fitted area, the more knots may be allowed in the LSF method. For example, in an area larger than that occupied by the WPDN, Panofsky (1949) adopted two polynomials and pieced them together. However, at least four knots are required in each direction by the regular LSF splines package. As might be expected, the package allowed too much variation when applied to the WPDN data.

Based on the above tests, simple polynomials in x, y, z, and t (similar to one piece of a spline) have been used in the LSF method. There are some disadvantages when using polynomials as basis functions as discussed by Daley (1991). For example, polynomials tend to approach infinite values at large distances and extrapolations become dangerous. To alleviate this problem, all of the numerical results are taken only in the region over the central part of the United States outlined with a solid line in Fig. 1. This region is hereafter referred to as "the window". As evident from Fig. 1, there are a few WPDN stations outside the window to guarantee that the polynomial evaluations are interpolations in the area where the data are used. It is also the case that the degree of polynomial functions is reduced by the differentiation process. However, the highest derivative terms in the vorticity equation are the second derivatives of the velocity. In this study, the degree of polynomial basis functions is chosen to be high enough to adequately resolve the large-scale vorticity variabilities over the window. Although high degree polynomials usually result in large condition numbers, the use of low degree polynomials in the LSF method does not create severe numerical problems (Carl de Boor and Heinz Kreiss, personal communications). Discussions of basis functions chosen for the 4-D LSF method and the associated condition number are given in Section 3.

Having decided to use polynomial basis functions in the 4-D LSF method, its mathematical formulation can be written as follows. An observational field, $b(x, y, z, t)$, is expressed as a sum of four-dimensional polynomials in the form similar to that used by Panofsky (1949):

$$b(x, y, z, t) = \sum_{i,j,k,l} c_{i,j,k,l} x^i y^j z^k t^l \quad (i+j+k+l \leqslant N), \tag{2}$$

where x, y, and z are independent variables in the longitudinal, latitudinal, and vertical directions, respectively, and t is time. A four-dimensional polynomial basis function is denoted as $x^i y^j z^k t^l$ with the associated coefficient denoted as $c_{i,j,k,l}$. The degree of a multi-dimensional polynomial is defined as the maximum power of any independent variable in the polynomial. In this study, the observed data* are approximated by polynomials of degree less than or equal to 4, i.e., $N = 4$.

* Since there are no direct measurements for vorticity and divergence, the WPDN wind measurements are used in the 4-D LSF method.

The mathematical formulation of (2) can be rewritten as the following $m \times n$ matrix equation

$$AC = B, \tag{3}$$

where the coefficients to be determined are denoted by C, a $n \times 1$ column vector. The $m \times n$ matrix A is determined only by the locations of the observations, and the $m \times 1$ column vector B is calculated from the observed data. An LSF problem is meaningful only if $m > n$, i.e., $AC = B$ is an overdetermined system that in general has no exact solution. Thus, an LSF solution is the solution to the problem min $\|AC - B\|_2^2$, where $\|\cdot\|_2$ is the l_2 norm. The coefficients of the fit, C, can be determined by standard methods for LSF problems, e.g., the Q–R factorization* (Golub and Van Loan, 1983). The matrix factorization problem in terms of the limited memory and speed of the computer are trivial in this study. The 4-D LSF method when applied to the WPDN data solves a matrix of $10^4 \times 10^2$ in only a few minutes of CPU time on a work station.

The maximum polynomial degree is determined by the number of observations and desired data variability in the area of interest. The number of observations in each direction should be large enough to resolve the data variability in that direction. For example, the current 12-h rawinsonde (RAOB) data provides only two observational points per day to fit the variability in time. In contrast, the hourly averaged three dimensional atmospheric wind profile from the WPDN provides 24 observational points over the same period. The high temporal resolution WPDN data provides sufficient data in time for the basis functions to accurately describe the large-scale temporal variability. The large volume of WPDN data is used to reduce observational noise in the 4-D LSF analysis.

* LSF solution to min $\|AC - B\|_2^2$ can be obtained by either of the following two ways. One is to use a standard matrix solver to solve the normal equations, $A^TAC = A^TB$, where A^T is the transpose of A. The other is to solve $AC = B$ for C using the Q–R factorization. The condition number of the former method is approximately the square of that in the latter method. Therefore, the authors describe the LSF method in $AC = B$ form, rather than the normal equations.

3. Analytic case

An analytic solution is useful in demonstrating how the selection of the variation of the basis functions is used to separate the signal from the noise in the data. The analytic solution derived in LB contains spatial and temporal variations resembling large-scale atmospheric motions and satisfies the vorticity equation when proper terms are added. This analytic solution is used to examine the sensitivity of various basis functions in the 4-D LSF method. Different sets of basis functions are tested using the analytic solution with and without random errors. Based on the error sensitivities, a set of basis functions is chosen for the 4-D LSF method. The LSF method is also applied to the WPDN data and results are compared independently with the NMC GDAS data as shown in the next section.

3.1. Analytic solution

The analytic solution, whose detailed formulation can be found in LB, is defined by the streamfunction (Ψ) and the velocity potential (χ) that are expressed by:

$$\Psi(x, y, z, t) = -u_0 y + \Psi_0(F_{xx}G + FG_{yy})\, H(z), \tag{4}$$

$$\chi(x, y, z, t) = -\frac{fu_0}{g\tilde{\theta}} \Psi_0 F_x G H_{zz}(z), \tag{5}$$

where u_0, the mean flow, is chosen as $10\ \mathrm{m\,s^{-1}}$, and Ψ_0, a normalization factor, can be selected to give a reasonable size of velocity. Coriolis and static stability parameters are defined as $f = 2\Omega \sin\phi$ and $\tilde{\theta} = (1/\theta)\, \partial\theta/\partial z$, respectively. The functions $F(x - x_0 - u_0 t)$, $G(y - y_0)$, and $H(z)$ represent the dependence of the streamfunction on x, y, and z, respectively. The point (x_0, y_0) is the center of the analytic solution.

For the horizontal distribution, $F(x - x_0 - u_0 t)\, G(y - y_0)$, Gaussian functions are adopted as follows:

$$F(x - x_0 - u_0 t)\, G(y - y_0) = \exp\left[-\left(\frac{x - x_0 - u_0 t}{r_e}\right)^2\right] \exp\left[-\left(\frac{y - y_0}{r_e}\right)^2\right] = \exp\left[-\frac{(x - x_0 - u_0 t)^2 + (y - y_0)^2}{r_e^2}\right],$$

where r_e is the e-folding factor and is chosen as 2×10^6 m for the large-scale motion. The temporal variation of the analytic solution is thus determined by

$$\frac{\partial F(x-x_0-u_0 t)}{\partial t} = 2u_0 \left(\frac{x-x_0-u_0 t}{r_e^2}\right) \times F(x-x_0-u_0 t).$$

For the vertical distribution, $H(z)$, is a cosine function with its argument normalized by the height of the atmosphere, $z_T = 12$ km. Given the streamfunction and the velocity potential, the rest of the dynamical fields including velocity, vorticity, and divergence can be determined. The spatial and temporal variations in the analytic solution are similar to large-scale atmospheric motions. For example, the vertical variation in the analytic solution is a cosine function that gives reverse circulations in the lower and upper atmosphere similar to the internal mode circulation commonly observed in atmospheric motions. The temporal variation is determined by the translation of the three dimensional analytic solution with the mean wind, i.e., 10 m s^{-1} in this case.

Random errors are also added to the analytic solution to test the sensitivity of the 4-D LSF method to the presence of errors in the data. The random wind errors are simulated by a computer-based random number generator that generates a random number between 0 and 1. For example, the perturbed u^e and v^e are defined as

$$u^e(x, y, z, t) = u^a(x, y, z, t) \times \{1 + \alpha[r_1(x, y, z, t) - 0.5]\},$$

$$v^e(x, y, z, t) = v^a(x, y, z, t) \times \{1 + \alpha[r_2(x, y, z, t) - 0.5]\},$$

where $(\ )^a$ are the horizontal wind components without random errors. Random numbers, $r_1(x, y, z, t)$ and $r_2(x, y, z, t)$, range from 0 to 1. For example, $\alpha = 0.5$ and 0 imply an analytic wind field with and without 25 % random errors, respectively. It is noted that real observational errors are not necessarily random and can be spatially and temporally correlated. However, random error is not used to create real observation error, rather it is used to test the sensitivity of the 4-D LSF and vorticity methods to errors in the data.

3.2. Sensitivity of basis functions

The choice of basis functions follows the pioneering study of Panofsky's (1949) two-dimensional LSF experiments. Note that the lateral areas covered in Panofsky (1949) are on the order of 10^6 square miles, similar in size to the areas covered by the WPDN. The following sets of basis functions are used to determine the effect of the amount of variation in the basis functions in the horizontal, vertical and temporal dimensions. These basis functions, listed as Experiment A–E in Table 1, allow different spatial and temporal variations in the analyzed field by gradually removing a number of polynomials from the 4th degree polynomial basis functions.

Experiment A includes all of the polynomial basis functions of the 4th degree or less, i.e., $x^i y^j z^k t^l$ with $i+j+k+l \leq 4$. In this experiment, there are a total of 70 polynomial basis functions. In the experiment B, the 4th degree polynomial functions in a single variable, i.e., x^4, y^4, z^4, t^4, that tend to fit localized data noise, are removed. Since the number of profiler stations in the horizontal are limited, the polynomial functions which include only x and y terms, i.e., x^3y, xy^3, x^2y^2 are also removed to reduce the horizontal variation allowed. To examine the effect of temporal variability, the largest time variation in the experiment B is reduced from t^3 to t^2 to form experiment C. Specifically, the terms xt^3, yt^3, zt^3 are removed from B for experiment C. Similarly, to investigate the effect of vertical variation, the terms xz^3, yz^3, tz^3 are deleted from experiment C to form experiment D. These basis functions that allow z^3 vertical variations in the LSF method are very important

Table 1. *Maximum power of independent variables and terms omitted in basis functions for experiments A–E*

	x	y	z	t	Terms omitted
A	4	4	4	4	
B	3	3	3	3	x^4, y^4, z^4, t^4, x^3y, xy^3, x^2y^2 omitted from A
C	3	3	3	2	xt^3, ut^3, zt^3 omitted from B
D	3	3	2	2	xz^3, yz^3, tz^3 omitted from C
E	3	3	3	1	x^2t^2, y^2t^2, z^2t^2, xyt^2, xzt^2, yzt^2 omitted from C

to properly fit reverse circulations in the lower and upper atmosphere. Finally, the time variation in experiment C is further reduced to form experiment E, i.e., the 6 terms, x^2t^2, y^2t^2, z^2t^2, xyt^2, xzt^2, yzt^2, are deleted from C for experiment E.

The above basis functions were tested with the analytic solution initially centered east of station 27 (see Fig. 1 for the station location). The analytic vortex traveled 10 m s^{-1} eastward for 24 h and generated hourly vertical wind profiles at all WPDN stations. These irregularly-distributed analytic values were sampled every hour for 24 h at every kilometer in the vertical. The sampled analytic zonal and meridional wind values are fit by the 4-D LSF method with various basis functions. The LSF wind fields are used to compute the vorticity (ζ) and divergence (δ_ζ) from the vorticity method as described previously. These results are compared with the analytic solution to quantify the accuracy in the fit of wind, vorticity (first derivative), and divergence (second derivatives) derived from the vorticity method. These experiments are performed with the exact analytic wind values, and are repeated with random perturbation errors to show the variation in the basis functions in providing the proper balance between truncation and simulated observational errors.

Measures of the accuracy of the various experiments are made by computing the relative l_2 norm, i.e., relative root-mean-square (rms) error, between the LSF values and the analytic solution at verification points in the window area shown in Fig. 1. These verification points are chosen as the grid points in the analytic case and the WPDN observational points in the profiler data case. For example, the relative l_2 error for a vector, $V = (u, v)$, is expressed as follows:

$$\mathrm{err}(V) = \frac{\| V^{\mathrm{a}} - V^{\mathrm{c}} \|}{\| V^{\mathrm{a}} \|}, \tag{6}$$

where $\| \ \|$ denotes the l_2 norm. The analytic and computed values are represented as V^{a} and V^{c}, respectively. Note that the mean wind, u_0, is subtracted from V^{a} and V^{c} in the computation of eq. (6) in the analytic case.

Table 2 shows the relative l_2 errors in V, ζ, and δ_ζ for the 4-D LSF method with and without random errors for various basis functions. Without random errors, the last error appears in A, while the errors with the relatively low degree polynomials in D and E are noticeably increased. The differences of the errors among the experiments A, B and C for $\alpha = 0$ are small and are only obvious in the second derivative quantities, δ_ζ. In contrast, when the vertical variation decreases from z^3 in C to z^2 in D, the fitting errors increase substantially. For example, the error in V increases from 2.6 % in C to 12.1 % in D because the highest degree of z in the latter is the second degree (z^2) which is not sufficient to resolve the vertical variation of the cosine function in the analytic solution. Errors of V and ζ in E are similar to those in C. However, the error in δ_ζ increases from 4.5 % in C to 46.1 % in E when the degree of the basis functions in time decreases because the basis function t in the latter is not able to resolve the vorticity evolution. Without random error it is clear that the higher the degree of the polynomial basis functions, the smaller the error. However, this is no longer true when random errors are included in the data.

Table 2. *The l_2 errors of the 4-D LSF with various basis functions in the model grid points for the analytic and perturbed wind fields*

	Analytic ($\alpha = 0$)			Perturbed ($\alpha = 0.5$)		
	err(V) (%)	err(ζ) (%)	err(δ_ζ) (%)	err(V) (%)	err(ζ) (%)	err(δ_ζ) (%)
A	2.5	2.9	3.8	5.1	5.4	18.9
B	2.5	2.9	4.4	4.8	4.9	17.8
C	2.6	2.9	4.5	4.8	4.9	17.0
D	12.1	12.9	13.9	12.5	13.2	23.5
E	4.2	5.0	46.1	5.7	6.3	48.8

When random errors are included, the errors in V, ζ, and δ_ζ in Table 2 increase in proportion to the size of the random errors. This shows that the LSF solution not only tries to fit the analytic solution, but also adjusts to variations caused by random errors. Thus, it is not necessarily the case that higher degree basis functions give better results as they do in the case of no random errors. In other words, there is a trade-off in choosing the degree of basis functions in the LSF method between the true data variability and observational noise. Table 2 shows that the smallest fitting error occurs in C when random errors are included. Without random errors, basis functions in C fit the analytic solution within a few %, i.e., very close to those obtained by including higher degree polynomial basis functions in A and B.

These experiments show that when the random errors are included, the basis functions in C adjust to these errors to a lesser degree than those in A and B.

Based on the above experiments with analytic values generated at the Profiler Network stations, the polynomial functions in experiment C are chosen as the basis functions to fit the WPDN data. Note that these basis functions include the same polynomials in the horizontal, i.e., x^3 and y^3, as those used in Panofsky (1949) because the lateral areas in that study are similar in size to those covered by the WPDN. These basis functions accurately fit the analytic solution within a few % with or without random errors. Even though these basis functions are non-orthogonal, the condition number of the matrix A in (3) is on the order of 10^3 which is sufficiently small even for a 32-bit computer. Thus, it is not necessary to apply the Gram-Schmidt process to transform the non-orthogonal functions into orthogonal ones.

The above results were obtained with the irregularly distributed profiler stations. Numerical experiments with regularly distributed data were also carried out to examine the effect of the data irregularity on the 4-D LSF results. In the regularly distributed data experiments, the analytic values are generated every 250 km in the window. These regularly distributed values were fit with the 4-D LSF method. The results between the irregular and regular cases are similar. This is because the spacing between the WPDN profiler stations in the window is roughly the same even though the stations are not on a uniform grid. The 4-D LSF experiments are also repeated with the sampling of the irregularly distributed data at every 12 h (observational interval for rawinsonde data). The results show large errors because there are not enough data points for the basis functions to resolve the temporal variations. The hourly l_2 errors of the 4-D LSF method for the analytic solution were also examined. The l_2 errors are quite uniformly distributed over the 24-h period. The errors at the end-hour of the analysis period do not appear to be noticeably larger than those at other times.

4. WPDN results

After tests with the analytic solution, the 4-D LSF method was applied to a real case with WPDN data. In this case, the synoptic weather situation over the window region is dominated by large-scale flows with a deep trough in the north and a high pressure in the south. Since the focus is only on large-scale motions, the following 4-D LSF large-scale divergence and vorticity are compared with the GDAS longwave components. The WPDN data used in the 4-D LSF consist of hourly vertical wind profiles for 24 h starting from 12 UTC of September 9th to 11 UTC on September 10, 1992. The GDAS analysis data used for comparisons were taken over the same period at 6-h intervals, i.e., 12 and 18 UTC on the 9th and 00 and 06 UTC on the 10th.

4.1. Data

The WPDN provides vertical wind profiles measured by 3-beam Doppler radars directed upward from the profiler sites every six minutes. The 6-min wind measurements are averaged over an hour to reduce the effect of small-scale turbulence on the wind measurements. The hourly averaged data are subjected to an automated quality control procedure (Miller et al., 1994). The accuracy of wind profiler measurements has been compared with rawinsonde and Doppler lidar wind measurements. The relative rms differences between the profiler and the rawinsonde and lidar winds are several m s^{-1} which is within the uncertainty involved in the comparisons (Van de Kamp, 1988).

Winds are measured by the profilers with a vertical resolution of 250 m from a minimum height of 500 m above the ground level (AGL) to a maximum height of 16.25 km (AGL). The WPDN data are neither available below 500 m AGL nor reliable for the first gate or two (Stensrud et al., 1990). Therefore, the current WPDN observing system does not adequately observe planetary boundary layer (PBL) features. Due to the unavailability of the WPDN data in the planetary boundary layer (PBL), the data below 1.5 km are not included in the following 4-D LSF results.

The GDAS assimilates 12-h radiosonde, satellite derived temperature and cloud motion vectors, aircraft, buoys, ship observations. These assimilated data do not include WPDN hourly wind measurements. The GDAS data, archived at the National Center for Atmospheric Research (NCAR), includes the T-126, i.e., a triangular spectral resolution of 126 wavenumbers, spectral coefficients for the vorticity and divergence at 18 sigma levels. These coefficients are used in a conversion program to derive GDAS vorticity and divergence on a $1.125° \times 1.125°$ latitude-longitude grid. The GDAS zonal and meridional winds are also derived from these coefficients using the Helmholtz relation.

The GDAS wind, vorticity and divergence fields are compared with those derived from the vorticity and the 4-D LSF methods. Since comparisons of large-scale divergence may be obscured by GDAS high wavenumber spectral coefficients, it is desirable to remove the high wavenumber GDAS coefficients. All of the GDAS vorticity and divergence shown in the following are obtained by truncating at wavenumber 36 (T-36) whose smallest resolvable wavelength is roughly 1000 km in the mid-latitudes.

In the vertical, GDAS data are given on sigma surfaces, but the 4-D LSF method produces functional values in terms of the geographical height. In the horizontal, GDAS data are located in spherical coordinates while the 4-D LSF results are calculated in general stereographic coordinate (GSTC). (The GSTC formulation is included in the appendix). To bring the GDAS data to the location of the profiler sites for the comparisons, a bi-cubic interpolation in the horizontal and a cubic spline in the vertical were used. Different interpolation schemes gave similar results.

4.2. Numerical results

The WPDN 24-h measurements from 29 profilers are sampled for the 4-D LSF method at every hour and every kilometer starting from 1.5 km up to 16.25 km AGL. These wind measurements are projected onto the GSTC for the zonal and meridional winds which are then fit separately by the 4-D LSF method. The 4-D LSF wind fields are used to produce large-scale dynamic fields such as vorticity and divergence in the same manner as described in the analytic case.

Quantitative comparisons of the accuracy in the LSF and GDAS initial data are made using the

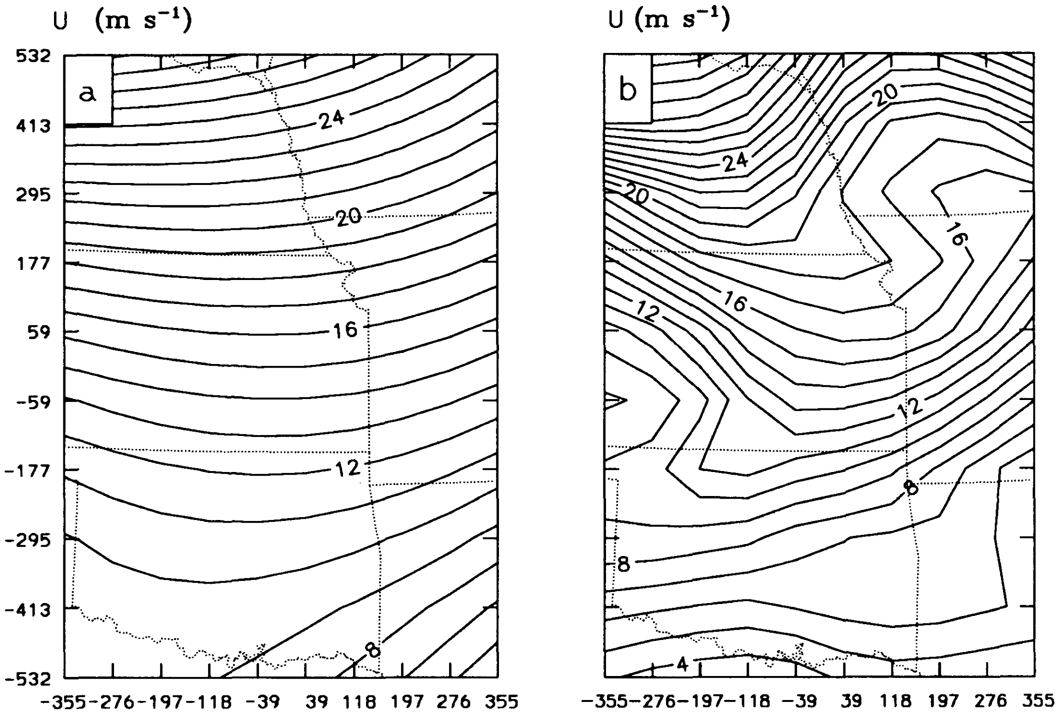

Fig. 2. The 500 mb zonal wind derived from (a) the 4-D LSF method and (b) the interpolated WPDN data at 06 UTC on 10 September. The contour interval is 1 m s^{-1}.

relative error defined in (6). Both the 4-D LSF and GDAS data are compared with the WPDN wind measurements. The relative error between the WPDN measurements and the LSF wind field is 25.1%, while for the GDAS T-36 and GDAS T-126 it is 25.9% and 26.4%, respectively. Note that the full and partial wavenumber spectra have similar rms differences relative to the WPDN observations. This is because the majority of the atmospheric kinetic energy resides in the large-scale motions (see, e.g., Fig. 1.4 in Daley, 1991). The zonal and meridional wind fields (not shown) derived from the 4-D LSF method are similar to those derived from the GDAS analysis.

The 500 mb zonal wind fields at 12 UTC on 9 September are used to illustrate the ability of the LSF method to remove observational noise or unresolved scale features. Fig. 2 shows the 500 mb zonal wind fields derived from the 4-D LSF method and interpolated WPDN data, respectively. Fig. 2b is obtained by using interpolation schemes to transfer the irregularly-distributed WPDN measurements to the GSTC grid at 500 mb. Since interpolation schemes provide interpolated values at observational points close to observed values, Fig. 2b essentially depicts the actual WPDN measurements at 500 mb. Comparing Figs. 2a and b shows that the wind speeds in these figures differ substantially over southwestern IOWA near station 13 (see Fig. 1 for the station location). These wind fields are further compared to the GDAS analysis zonal flow (not shown). It is found that the zonal wind fields derived from the LSF and GDAS analyses are similar. The wind speed obtained from the interpolation over southwestern IOWA in Fig. 2b is noticeably smaller than those in LSF and GDAS analyses. In other words, this relatively small wind does not appear in the GDAS analysis which does not assimilate WPDN data. This indicates that wind measurements near 500 mb at station 13 are likely either unresolved features or observational errors.

The interpolation procedure was repeated without the data from station 13 and the result is shown in Fig. 3. This figure is more similar to those derived from the LSF and GDAS than Fig. 2b. This demonstrates that wind measurements near 500 mb at station 13 are inconsistent with those in the LSF and GDAS analyses. These inconsistent measurements, reported only by station 13, noticeably change the flow pattern near the station when traditional local interpolation schemes are used. However, even though these inconsistent measurements are included in the LSF analysis, their effects on the 4-D LSF results are greatly reduced. These inconsistent measurements may be observational errors or unresolvable scale features. Since it is very difficult to distinguish unresolvable small scale features from observational errors, the unresolvable fluctuations are treated as noise and are smoothed out by the smoothing mechanism in the LSF method.

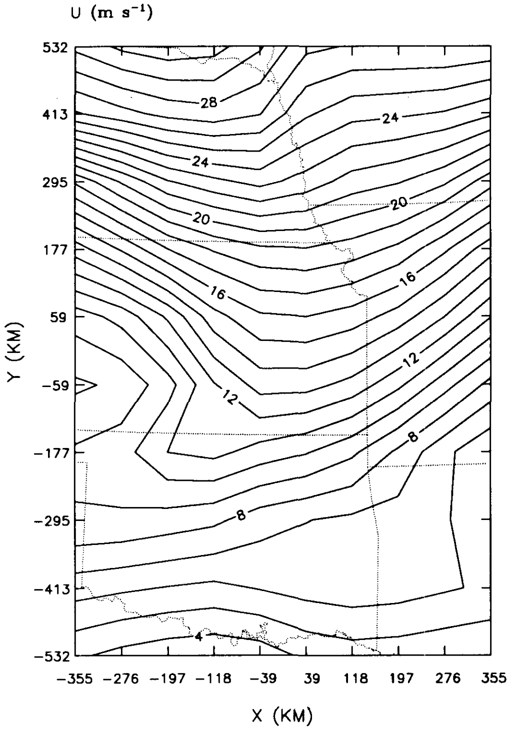

Fig. 3. Same as Fig. 2b, except data from station 13 are not included in the interpolation. The contour interval is $1\ \mathrm{m\,s^{-1}}$.

Fig. 4 shows the 300 mb divergence fields derived from the kinematic and vorticity methods at 06 UTC on 10 September. A positive sign (solid contours) means divergence and a negative sign (dashed contours) denotes convergence. The divergence fields derived from the kinematic and vorticity methods are very different. For example, Fig. 4a is dominated by divergence (positive sign) with the maximum divergence located at the

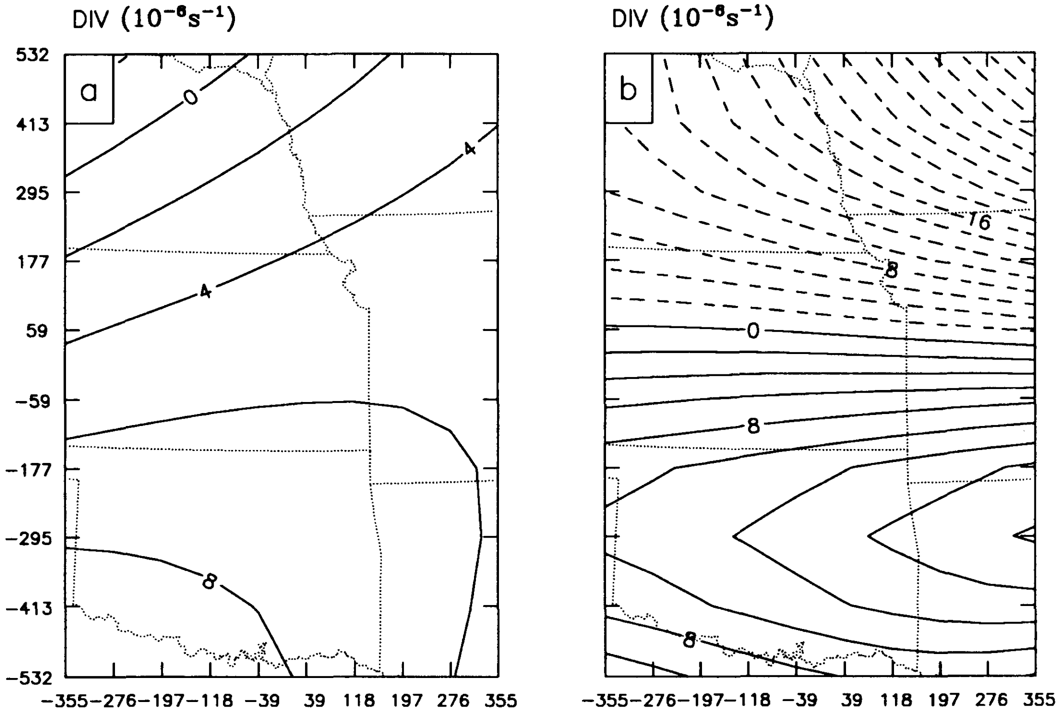

Fig. 4. The 300 mb divergence fields at 06 UTC derived from the (a) kinematic method and (b) vorticity method. The contour interval is $2 \times 10^{-6}\,s^{-1}$.

southwestern corner of the domain, while in Fig. 4b divergence and convergence are located at the southern and northern parts of the domain, respectively. Since divergence is not a directly observed quantity, the divergence fields derived from the kinematic and vorticity methods are compared with that derived from the GDAS divergence shown in Fig. 5. The divergences derived from the vorticity method and GDAS are similar, but that is not the case for the kinematic method.

The 300 mb vorticity fields derived from the LSF and GDAS data for 06 UTC are shown in Figs. 6a and b, respectively. The following comparisons are made on the relative vorticity rather than absolute vorticity because the former depends solely on velocity fields and the latter is dominated by the Coriolis parameter, f. The vorticity fields in Figs. 6a and b are positive in the north and negative in the south. Since GDAS vorticity is the product of model forecasts and observational data, it is not obvious whether the vorticity differences come from the model dynamics/physics or from the data insertion procedure in the 4-DDA. Due to the temporal roughness of the observational data, the above comparison of vorticity at a given time may be obscured by temporal variations in the vorticity.

An example of the temporal variation in the vorticity is given in Figs. 7 and 8. These figures show the 4-D LSF and GDAS 700 mb vorticities derived at 12, 18, 00, and 06 UTC. Comparisons of vorticities in Figs. 7a–d, respectively, with those in Figs. 8a–d show that the vorticity derived from these two methods are somewhat different. For example, Fig. 8a shows positive vorticity values over the border of Kansas and Nebraska which are not found in Fig. 7a. These differences can be caused by different temporal or spatial (or both) variations in the two analyses. In order to separate variations in space from those in time, the GDAS vorticities were smoothed in time and compared

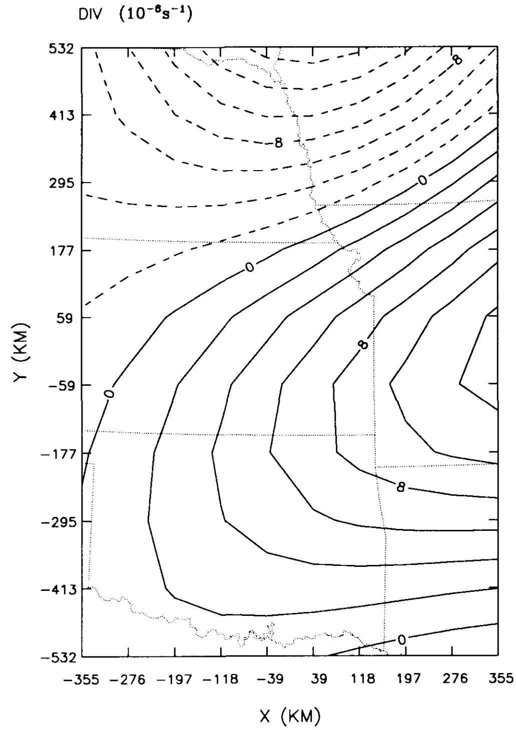

Fig. 5. The 300 mb divergence fields at 06 UTC derived from the GDAS analysis data. The contour interval is $2 \times 10^{-6}\ s^{-1}$.

with the smoothed LSF vorticity. The most straightforward way to smooth the LSF and GDAS vorticities in time is to average their respective vorticities. The vorticity fields shown in Figs. 9a and b, are averaged from Figs. 7 and 8, respectively. It is obvious that the averaged vorticities derived from the 4-D LSF method and GDAS analysis are very similar, despite their differences at a given time. This shows that the 4-D LSF and GDAS analyses produce similar vorticity spatial variations. Even though their temporal variations are somewhat different, these differences are evidently small and can be averaged out. In other words, the smooth part of vorticity in the 4-D LSF and GDAS analysis data are similar.

Since the WPDN data variabilities may differ from those in the analytic solution, the sensitivity of basis functions in experiments *A* to *E* shown previously with the analytic solution were repeated with the WPDN data. The LSF horizontal winds with different basis functions have very similar rms errors relative to the WPDN wind measurements. The vorticity fields with the basis functions in the experiment of *A*, *B*, *D* and *E* are shown, respectively, in Figs. 10a–d. These vorticity fields strongly resemble Fig. 6a derived from the basis functions of the experiment *C*. The divergence fields (not shown) derived from the vorticity method with different basis functions are also very similar. The basis functions used in *A* produce a larger divergence. However, the patterns are similar to the others. These results are consistent with those in the analytic case that more variation in basis functions picks up more noise which increases size of derivatives. Note that the choice of basis functions has less effect on the analyzed WPDN data than the analytic solution because the spatial and temporal variations in the data are less in the former than the latter. For example, the WPDN case examined in this study appears to have less vertical variation than the cosine function contained in the analytic solution.

5. Conclusions

The vorticity and 4-D LSF methods have been developed to utilize high temporal resolution WPDN wind measurements to derive dynamical fields, in particular the large-scale divergence, over a limited-area domain. The vorticity method computes the large-scale horizontal divergence based on the 4-D LSF wind and vorticity analyses deriving from the irregularly distributed WPDN hourly data. The hourly data are essential in providing temporal data variabilities for the 4-D LSF method and in computing the vorticity tendency for the vorticity method. The irregularity of the WPDN sites does not have a significant impact on the 4-D LSF results because the spacing of the profiler stations is fairly constant.

The vorticity and 4-D LSF methods are tested with an analytic solution, and then are applied to the WPDN data over a 24-hour period. In the analytic test case, these two methods accurately reproduce the analytic solution with or without random errors. Relative to the WPDN data, the error in the 4-D LSF wind field is close to that of the NMC GDAS assimilated data. The 4-D LSF method utilizing the large amount of WPDN data effectively removes observational noise or unresolvable scale features. The sensitivity of basis

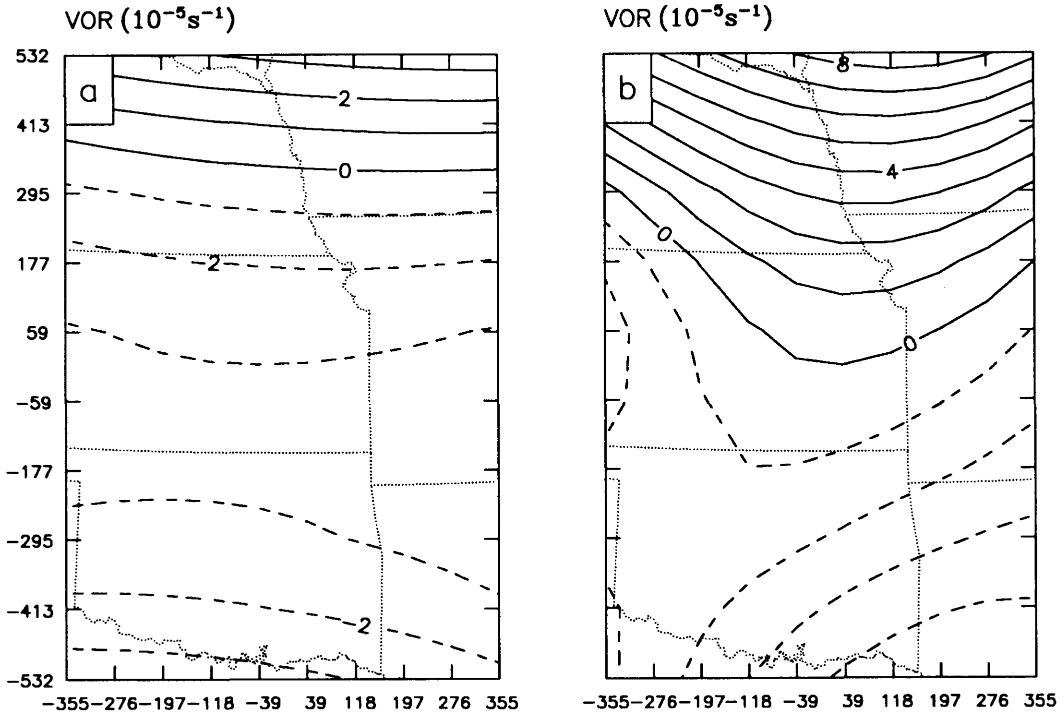

Fig. 6. The 300 mb vorticity fields at 06 UTC derived from (a) the 4-D LSF method and (b) the GDAS data. The contour interval is $1 \times 10^{-5}\,\mathrm{s}^{-1}$.

functions in the LSF method are studied with an analytic solution as well as real data. It is shown that the 4-D LSF results are not sensitive to the choice of basis functions as long as they include reasonable variations to resolve data.

The large-scale horizontal divergences derived from the vorticity method, GDAS data, and kinematic methods were compared. The large-scale divergence derived from the former two methods are similar, while that calculated from the last method shows little resemblance to the others. These results are consistent with the LB analysis that shows the vorticity method is less susceptible to small observational errors in deriving the large-scale divergence than the kinematic method. Although the vorticities derived from the 4-D LSF method and GDAS differ slightly at an instantaneous moment, their smooth parts are similar.

Comparisons of the GDAS data with those derived from the 4-D LSF and vorticity methods provide an independent check for these two analyses. These two analyses show similar results, although the result in the latter analysis come from hourly wind measurements, and the former analysis is produced by the assimilation model with 6-h data assimilation intervals. This consistency shows that the 4-D LSF and vorticity methods in conjunction with hourly WPDN data are able to produce reliable large-scale dynamic fields including wind, vorticity and divergence. The results obtained in this study are encouraging. This initial study is a large-scale case without condensational heating involved. Similar experiments with physically more complicated synoptic situations will be studied in the future.

6. Acknowledgments

The authors would like to thank Dr. Stanley Barnes for his helpful comments during the internal scientific review process. We are grateful to Dr. Roger Daley, Dr. Sundström, and the

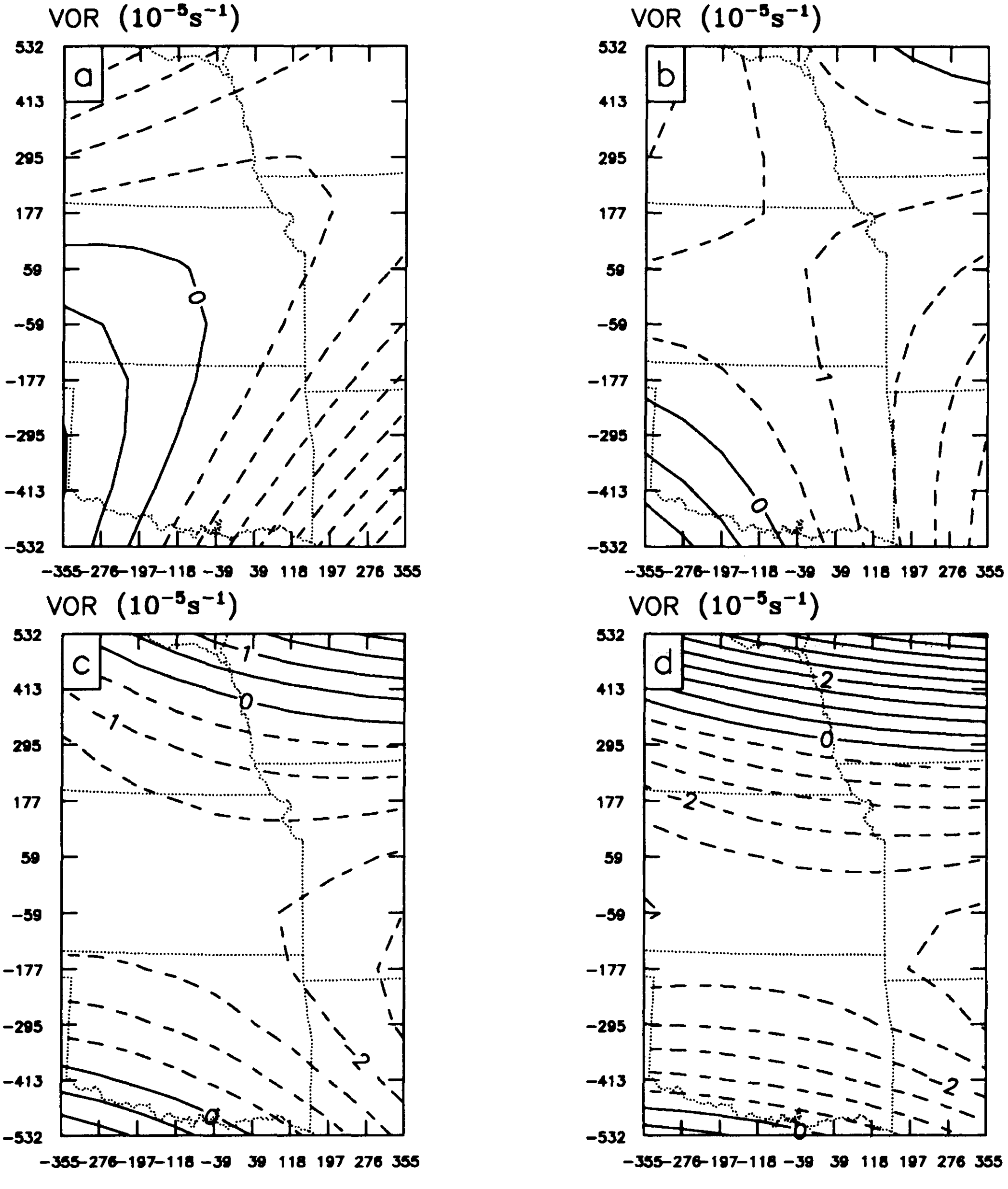

Fig. 7. The 700 mb vorticity fields derived from the 4-D LSF method at 4 different UTC times. The figures (a), (b), (c), and (d) are vorticity fields derived at 12 and 18 UTC on 9 September, and 00 and 06 UTC on 10 September, respectively. The contour interval is $5 \times 10^{-6}\ s^{-1}$.

Tellus A/47/5:1-26

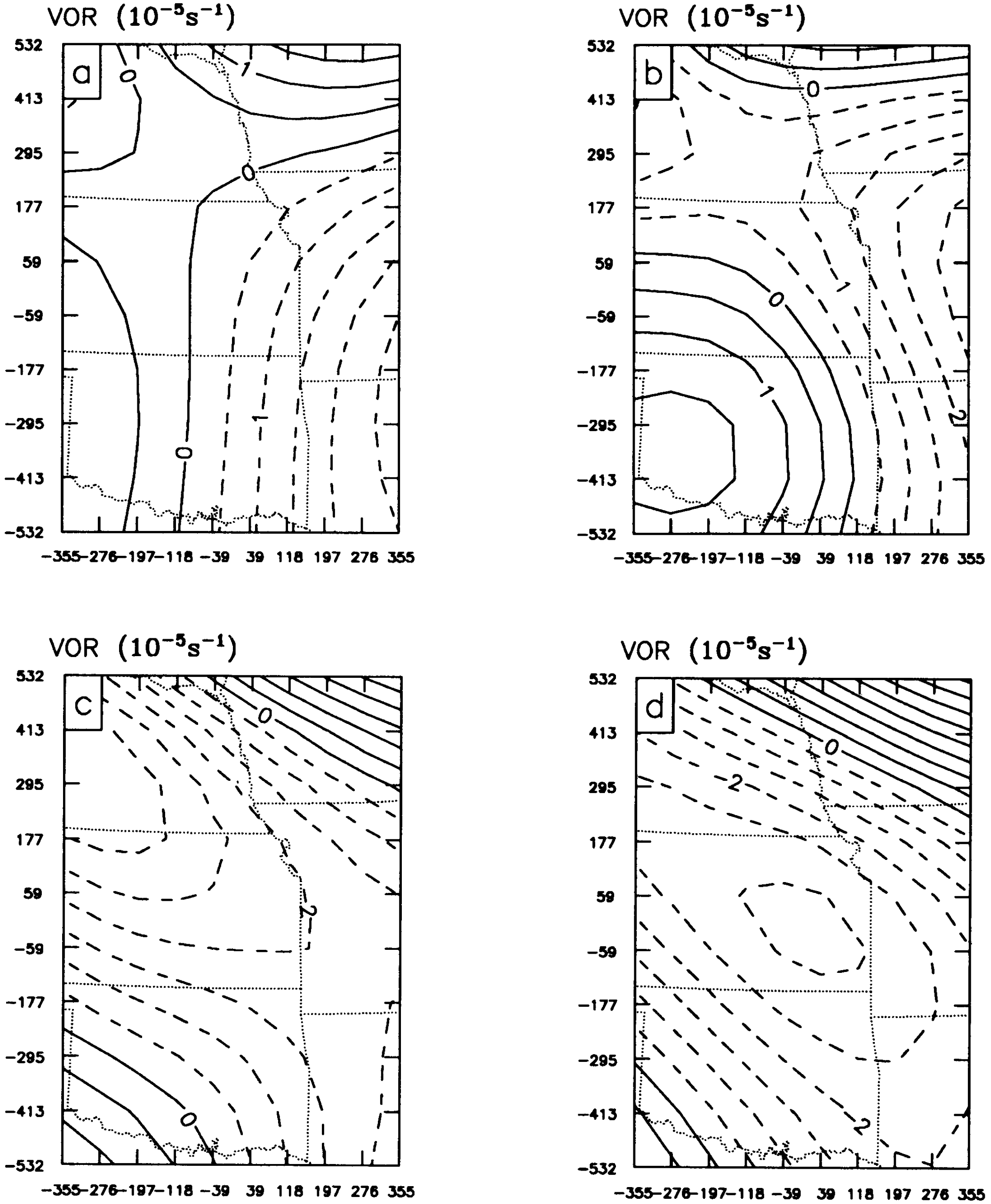

Fig. 8. Same as Fig. 7, except for the GDAS analysis data. The contour interval is 5×10^{-6} s^{-1}.

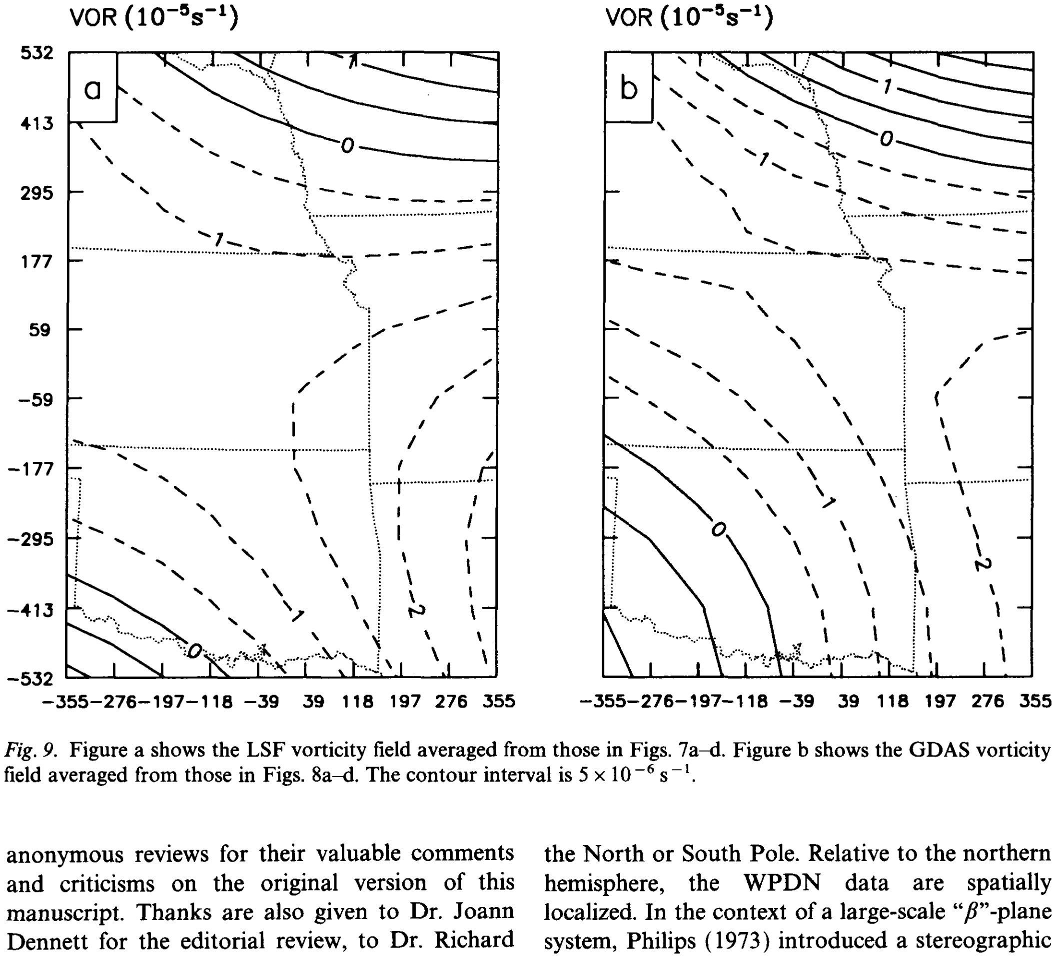

Fig. 9. Figure a shows the LSF vorticity field averaged from those in Figs. 7a–d. Figure b shows the GDAS vorticity field averaged from those in Figs. 8a–d. The contour interval is $5 \times 10^{-6}\ s^{-1}$.

anonymous reviews for their valuable comments and criticisms on the original version of this manuscript. Thanks are also given to Dr. Joann Dennett for the editorial review, to Dr. Richard Valent for providing us with thin-plate and regular LSF spline packages, and to Dennis Joseph and Steve Worley for their help in obtaining NMC analyses data from the NCAR archives.

7. Appendix

General stereographic coordinate

In numerical weather prediction and analysis on a regional area, it is useful to map the earth's surface, which is assumed to be a sphere, onto a plane. One such mapping often used in numerical weather prediction models is the polar stereographic projection. However, its mapping factor, the ratio of the distance between two points on the map and on the sphere, increases as the point of interest moves away from the projection point, i.e., the North or South Pole. Relative to the northern hemisphere, the WPDN data are spatially localized. In the context of a large-scale "β"-plane system, Philips (1973) introduced a stereographic projection similar to the polar stereographic projection with the tangent plane located at the point of longitude, $\lambda = 0$, and latitude, $\theta = \theta_0$, where θ_0 can be placed at mid-latitude to reduce the mapping factor. However, in a regional model, the center of the model domain may not be at the Greenwich line, i.e., $\lambda = 0$. In order to keep the map factor close to 1 over the profiler network, the WPDN data are projected onto the GSTC whose projection point is located near the center of the WPDN rather than the North Pole. Thus, the map factor is close to one in the region where data is dense and the vorticity equation is essentially that for Cartesian coordinates.

The GSTC is defined by projecting the surface of the earth onto a plane that is tangent at longitude λ_0 and latitude θ_0. The earth's surface is projected onto the GSTC by the antipode of the tangential

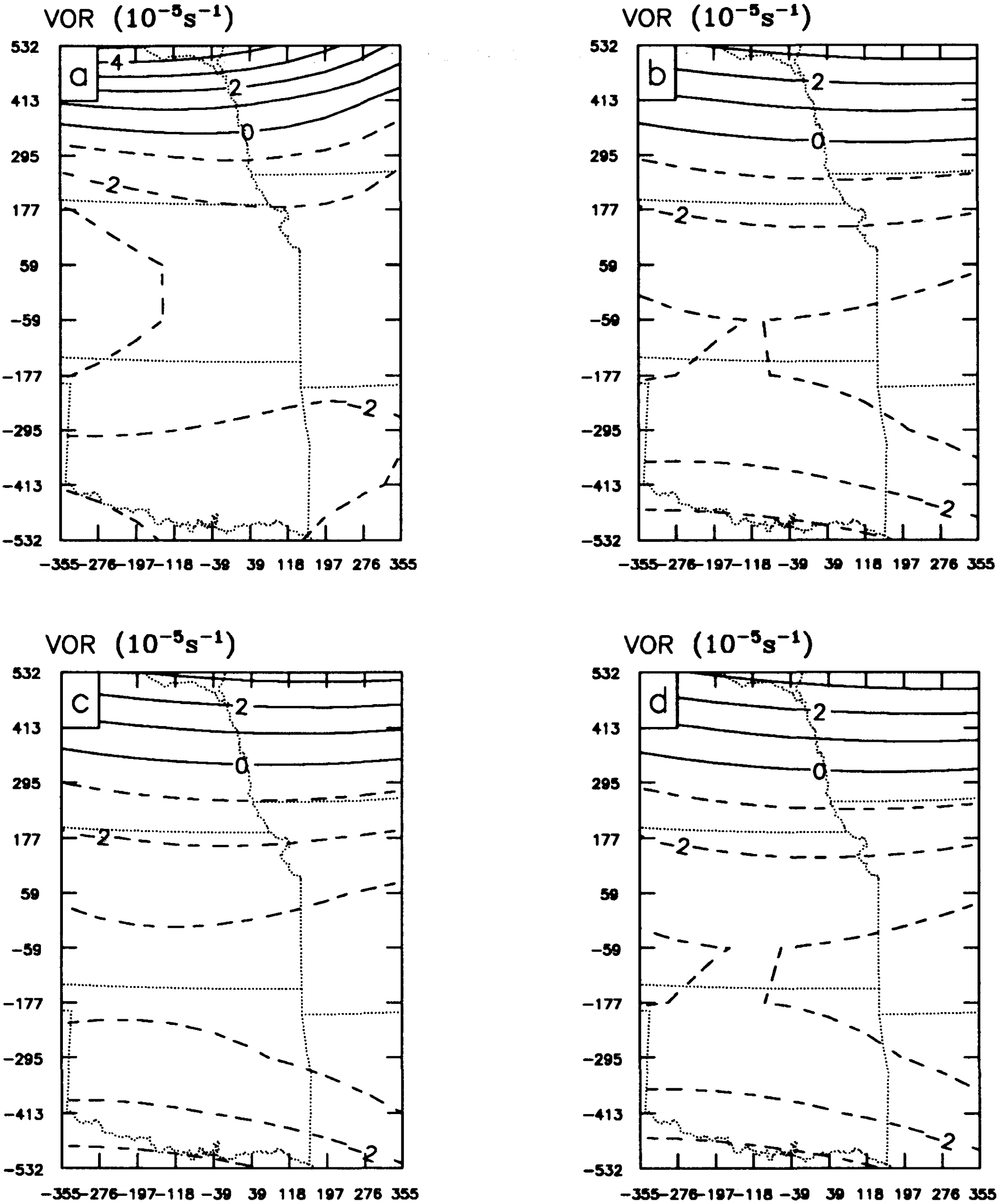

Fig. 10. The 300 mb vorticity fields derived from the 4-D LSF method with different basis functions. The figures (a), (b), (c), and (d) are derived using the basis functions in the experiment of A, B, D, and E, respectively. The contour interval is 5×10^{-6} s^{-1}.

point at $\lambda = \pi + \lambda_0$ and $\theta = -\theta_0$. The transformation between the spherical and GSTC is given by

$$x = m[a \cos \theta \sin(\lambda - \lambda_0)],$$

$$y = m[a(\sin \theta \cos \theta_0 - \cos \theta \sin \theta_0 \cos(\lambda - \lambda_0))],$$

$$m = \frac{2}{(1 + \sin \theta \sin \theta_0 + \cos \theta \cos \theta_0 \cos(\lambda - \lambda_0))} = \frac{4a^2 + x^2 + y^2}{4a^2},$$

where m is the map factor, a is the radius of the earth, θ is the latitude, and λ is the longitude. The center of the GSTC is at the tangent point where $x = 0$, $y = 0$. In the transformed system, the positive x-axis is directed towards the east of the origin along the latitudinal circle of $\theta = \theta_0$, and the y-axis is defined positive northward of the origin along the meridian $\lambda = \lambda_0$. When $\lambda = 0$, these transformation formulas are the same as those in Philips (1973).

REFERENCES

Beebe, R. G. and Bates, F. C. 1955. A mechanism for assisting in the release of convective instability. *Mon. Wea. Rev.* **83**, 1–10.

Bellamy, J. C. 1949. Objective calculations of divergence, vertical velocity and vorticity. *Bull. Amer. Meteor. Soc.* **30**, 45–49.

Bengtsson, L., Kanamitsu, M., Kållberg, P. and Uppala, S. 1982. FGGE 4-Dimensional Data Assimilation at ECMWF. *Bull. Amer. Meteor. Soc.* **63**, 29–43.

Browning, G. L., Kasahara, A. and Kreiss, H.-O. 1980. Initialization of the primitive equations by the bounded derivative method. *J. Atmos. Sci.* **37**, 1424–1436.

Daley, R. and Mayer, T. 1986. Estimates of global analysis error from the global weather experiment observational network. *Mon. Wea. Rev.* **114**, 1642–1653.

Daley, R. 1991. *Atmospheric data analysis*. Cambridge University Press, 457 pp.

Derber, J. 1987. Variational four-dimensional analysis using quasi-geostrophic constraints. *Mon. Wea. Rev.* **115**, 998–1008.

Dixon, R., Spackman, E. A., Jones, I. and Francis, A. 1972. The global analysis of meteorological data using orthogonal polynomial base functions. *J. Atmos. Sci.* **29**, 609–622.

Eliassen, A. and Hubert, W. E. 1953. Computation of vertical motion and vorticity budget in a blocking situation. *Tellus* **5**, 196–206.

Gilchrist, B. and Cressman, G. 1954. An experiment in objective analysis. *Tellus* **6**, 309–318.

Golub, G. H. and Van Loan, C. F. 1983. *Matrix computations*. The Johns Hopkins University Press, 476 pp.

Gu, C. 1989. *Rkpack and its applications: fitting smoothing spline models*. Technical Report No. 857, Department of Statistics, University of Wisconsin-Madison, 13 pp.

Halberstam, I. and Tung, S. L. 1984. Objective analysis using Hough vectors evaluated at irregularly spaced locations. *Mon. Wea. Rev.* **112**, 1804–1817.

Kanamitsu, M. 1989. Description of the NMC global data assimilation and forecast system. *Wea. Forecasting* **4**, 335–342.

Kasahara, A., Mizzi, A. P. and Donner, L. J. 1992. Impact of cumulus initialization on the spinup of precipitation forecasts in the tropics. *Mon. Wea. Rev.* **120**, 1360–1380.

Kreiss, H.-O. 1980. Problems with different time scales for partial differential equations. *Comm. Pure Appl. Math.* **18**, 399–439.

Lee, J. L. and Browning, G. L. 1994. Analysis of errors in the horizontal divergence derived from high temporal resolution of the wind. *Mon. Wea. Rev.* **122**, 851–863.

Lewis, J. 1972. An operational upper air analysis using the variational method. *Tellus* **24**, 514–530.

Miller, P. A., Schlatter, T. W., Van de Kamp, D. W., Barth, M. F. and Weber, B. L. 1994. An unfolding algorithm for profiler winds. *J. Atmos. Oceanic Technol.* **11**, 32–41.

Panofsky, H. 1949. Objective weather-map analysis. *J. Meteor.* **6**, 386–392.

Parrish, D. and Derber, J. 1991. The National Meteorological Center's spectral statistical interpolation analysis system. *Mon. Wea. Rev.* **120**, 1747–1763.

Philips, N. A. 1973. Principles of large-scale numerical weather prediction. *Dynamic meteorology*, ed., P. Morel. Reidel Publishing Co. 1–96, 622 pp.

Sardeshmukh, P. D. 1993. The baroclinic χ problem and its application to the diagnosis of atmospheric heating rates. *J. Atmos. Sci.* **50**, 1099–1112.

Sasaki, Y. 1969. Proposed inclusion of time variation terms, observational and theoretical, in numerical variational analysis. *J. Meteor. Soc. Japan* **47**, 115–124.

Sawyer, J. S. 1949. Large scale vertical motion in the atmosphere. *Quart. J. Roy. Meteor. Soc.* **75**, 185–188.

Schaefer, J. T. and Doswell, C. A. III, 1979. On the interpolation of a vector field. *Mon. Wea. Rev.* **107**, 458–476.

Stensrud, D. J., Michael, H. J., Kenneth, W., Howard, W. and Maddox, R. A. 1990. Operational systems for observing the lower atmosphere: importance of data sampling and archival procedures. *J. Atmos. Oceanic Technol.* **7**, 930–937.

Talagrand, O. and Courtier, P. 1987. Variational assimilation of meteorological observations with the adjoint vorticity equations. Part I. Theory. *Quart. J. Roy. Meteor. Soc.* **113**, 1311–1328.

Van de Kamp, D. W. 1988. *Principles of wind profiler operation*. Profiler Training Manual No. 1. NOAA/ERL/Forecast Systems Laboratory, Boulder, Colorado, 49 pp.

Wahba, G. and Wendelberger, J. 1980. Some new mathematical methods for variational objective analysis using splines and cross validation. *Mon. Wea. Rev.* **108**, 1122–1143.